Renewable Energy 180 (2021) 55–67

Contents lists available at ScienceDirect

Renewable Energy

journal homepage: www.elsevier.com/locate/renene

Dynamic aiming strategy for central receiver systems

N. Speetzen , P. Richter *

RWTH Aachen University, Research Group for Theory of Hybrid Systems, Department of Computer Science, Ahornstr. 55, 52074, Aachen, Germany

ARTICLE INFO

Article history:
Received 23 May 2021
Received in revised form
30 July 2021
Accepted 16 August 2021
Available online 19 August 2021

Keywords:
Dynamic aiming strategy
Central receiver system
Linear programming
Heuristic acceleration
Aim point management system

ABSTRACT

Aiming strategies in central receiver systems search for an optimal assignment between heliostats and aim point on the receiver surface. In this work, we develop an accelerated aiming strategy which can be used for dynamic scenarios such as short-term environmental influences. The strategy bases on the linear formulation of the problem. To achieve a performance close to real-time, we present several accelerations based on carefully chosen methods to reduce the problem size. The performance of different solvers is evaluated and the problem reduction is adjusted according to accuracy, prediction time and computational run-time. The accelerated aiming strategy is applied to central receiver systems with up to 8600 heliostats in a dynamic test scenario with cloud shadows passing over the heliostat field. The accelerated aiming strategy is effective enough to be used as a real-time control strategy.

1. Introduction

Central receiver systems are large scale power plants which make use of concentrated solar power to generate electric energy. The incoming solar irradiation is concentrated onto the central receiver and the heat is forwarded to a fluid which runs through pipes behind its surface. Afterwards a thermodynamic cycle transforms the energy into electric energy.

Depending on the total received solar power, the power plant operator adjusts the mass flow of the fluid in the receiver tubes such that the fluid is heated up to its desired outflow temperature. Based on the mass flow, an upper limit for the heat flux which the receiver can absorb without overheating can be precomputed in the form of an allowed flux distribution. Staying below these critical values is crucial to protect the receiver from taking permanent damage.

The aiming strategy problem searches for the heliostat alignment which yields the most power while staying below the allowed flux distribution.

In this work, we formulate the optimal aiming problem as integer linear program (ILP). With carefully chosen methods the problem size is reduced to decrease the run-time whereas maintaining a high degree of optimality. Several LP solvers are tested for the problem, using optimized solver settings. To the end, we show that the developed solver is able to solve a dynamic test case with passing cloud shadows over a large heliostat field in real-time.

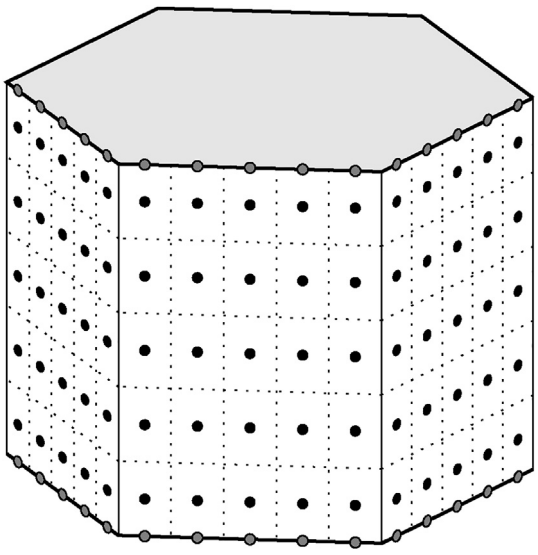

Fig. 1. Discretization of the external receiver surface. The filled dots (•) on the receiver surface represent the measurement points $\mathcal{M}^{\text{rec}}$, while the circular dots (◦) represent the measurement points on the heat shield $\mathcal{M}^{\text{shield}}$. As the flux concentration decreases with the distance to the receiver, the measurement points for the heat shield are chosen on the border of the receiver surface.

* Corresponding author.
E-mail address: pascal.richter@rwth-aachen.de (P. Richter).

https://doi.org/10.1016/j.renene.2021.08.060
0960-1481/

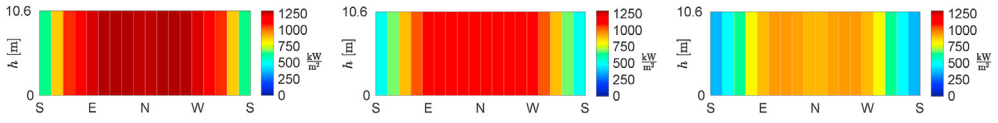

(a) Design point with flow intensity $\chi^{\text{intensity}} = 100\,\%$ (b) Flow intensity $\chi^{\text{intensity}} = 75\,\%$ (c) Flow intensity $\chi^{\text{intensity}} = 50\,\%$

Fig. 2. AFD maps for the *Gemasolar* central receiver system for different flow intensities $\chi^{\text{intensity}}$ on the receiver surface. The *Gemasolar* receiver consists of 18 panels.

1.1. State of the art

Aiming strategies for central receiver systems have been subject to prior research. The different approaches can be grouped into the group of specialized heuristics [1–6], metaheuristics [7–9], and solving a mixed-integer linear program formulation [10–14].

Dellin et al. [1] studied aiming strategy optimization as some of the first and propose fast heuristic aiming strategies, which aim to maximize the heat flux hitting the receiver while distributing the aim points of the heliostats in specific patterns. The heuristics are part of the DELSOL optics simulation software, an optimization software for the design of central receiver systems. García-Martín et al. [2] developed an iterative method to solve the aiming strategy problem by repeatedly changing heliostat aim points from high heat flux areas of the receiver to lower ones. This way, an almost uniform temperature is achieved across the surface. Kelly et al. [3] use a heuristic approach to approximate a predefined heat flux distribution across the receiver surface. Astolfi et al. [4] partition the heliostat field into small groups. This allows for independent solving of different subproblems with a heuristics, which reduces peak heat flux densities at the receiver by up to 15%. Garcia et al. [5] propose an agent-based multivariable model predictive control. Collado et al. [6] refine the approach of Astolfi et al. [4] by offering more exact aim point options, not only determining the best vertical aim position but using aim positions in two dimensions.

Belhomme et al. [7] propose an ant colony optimization metaheuristic. In comparison to a trivial solution, where all heliostats aim at the center of the receiver, an improvement of up to 10% is reached. Maximum allowed heat fluxes and spatial heat flux gradients are used as constraints in the optimization. Depending on the number of aim points a solution can be found within 38 min. By using a GPU the runtime of this optimization method could be reduced to a minute or less [9]. Besarati et al. [8] use a genetic algorithm to avoid peak heat fluxes.

More recent work tries to achieve solutions close to the global optimum while controlling the maximum error. Ashley et al. [10] define the optimization problem as an integer linear program (ILP). An even heat flux distribution is forced by constraining the allowed range of heat flux on each part of the receiver surface. Later, this strategy was extended to a continuous problem [11]. Richter et al. [12] develop a robust solution based on an ILP formulation. A desired flux distribution is introduced, which allows to solve for a specific heat flux distribution at the receiver. Several kinds of uncertainties are taken into account, as well as a limitation to spatial heat flux gradients. As follow-up, Kuhnke [13] extended the works of [10,12] by developing a mixed integer linear program formulation of the aiming strategy optimization including robustness to inaccuracies. A first step into an accelerated mixed integer linear program using heuristic formulations was done in Ref. [14].

Table 1
Overview of different ILP solvers and the used version for this investigation.

Solver	Licensing	Last update	Used version
Gurobi	Commercial and Academic	2020	9.0
CPLEX	Commercial and Academic	2020	12.9.0
SCIP	ZIB (academic)	2018	6.0.2
glpk	GNU GPL (free)	2018	4.65
lpSolve	GNU LGPL (free)	2016	5.5.2.5
COIN-OR	EPL (free)	2020	Cbc 2.10.4

1.2. Our contribution

To the knowledge of the authors, so far there does not exist any work on dynamic aiming strategies with changing weather conditions. In this paper, we focus on providing results in real-time while delivering the possibility to reach results close to the global optimum. Instead of approximating a solution based on heuristics or metaheuristics, the intention is to develop a reduced problem formulation and formulate it as an ILP. This adaptable approach delivers the possibility to drastically reduce the run-time while keeping the gap to the optimal solution as small as possible. In a dynamical test case our method will be tested for real-time use.

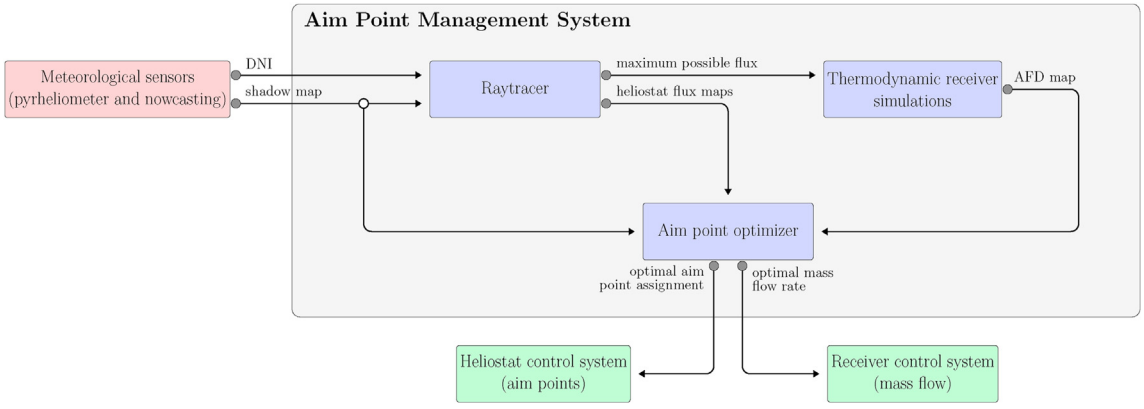

Fig. 3. Block diagram of the aim point management system with all components. At each instance of time the unit collects meteorological data from the sensors in the solar field, estimated the mass flow of the receiver system to load the corresponding AFD map, generates heat fluxes for each heliostat, runs the computation for an optimal aim point strategy and communicates with the control system of the receiver and the heliostat field.

Table 2
Average runtime in seconds for finding the optimal aim point assignment for a test case of the *PS10* and *Gemasolar* central receiver system using five different LP solvers. These runtimes have been achieved using an Intel i5 processor with 3200 MHz and 16 GB random-access memory.

Power plant	Configuration	Gurobi	CPLEX	SCIP	glpk	lpSolve	COIN-OR
PS10	Default configuration	2.89 s	1.7 s	28.73 s	176.43 s	>1 h	>1 h
PS10	irace configuration	2.87 s	0.89 s	25.08 s	86.83 s	>1 h	>1 h
Gemasolar	Default configuration	32.83 s	123.46 s	526.79 s	5242.45 s	>1 h	>1 h
Gemasolar	irace configuration	31.99 s	87.51 s	437.19 s	462.12 s	>1 h	>1 h

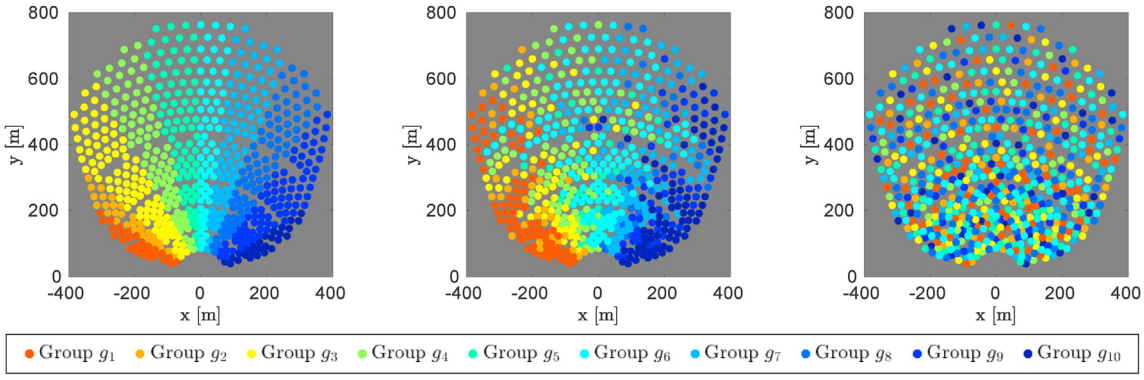

(a) angular dissimilarity function (b) combined dissimilarity function with 80 % angular and 20 % max-distance (c) max-distance dissimilarity function

Fig. 4. Grouping of heliostats for the *PS10* central receiver system into $n^{\text{groups}} = 10$ different groups. Heliostats within the same group are drawn with the same color.

1.3. Outline

The paper is structured as follows: In Section 2 the optical model for the computation of the heat flux is introduced. In Section 3 the underlying optimization problem is formulated as an integer linear program (ILP). To accelerate the solving process in Section 4 several reduction approaches are proposed and investigated. In Section 5 we apply the aiming strategies to three different central receiver systems. The accelerations are compared and together with five different solvers the run-time is optimized. Furthermore, a dynamic test case is used to investigate the quality of a real-time control. Finally, we draw in Section 6 a conclusion regarding the presented accelerated aiming strategies and give an outlook with possibilities to extend this work.

2. Optical model

This section introduces the optical components of a central receiver system which is needed to further describe the optimization problem for the aiming strategy.

2.1. Heliostats and receiver

A central receiver system consists of large field of *heliostats* which we denote as set $\mathcal{H}$. These heliostats collect the solar direct normal solar irradiation I_{DNI} from the *sun* and reflect the flux onto the surface of the *receiver*, where a heat transfer fluid inside the receiver is heated up. Any part of the receiver and the surrounding heat shield can only withstand a certain upper limit of heat without being permanently damaged. According to Kuhnke et al. [13] we discretize the receiver surface by a fine regular mesh of measurement points $\mathcal{M}^{\text{rec}}$ at which the allowed flux distribution is defined and on which we observe the arriving heat flux from the heliostats.

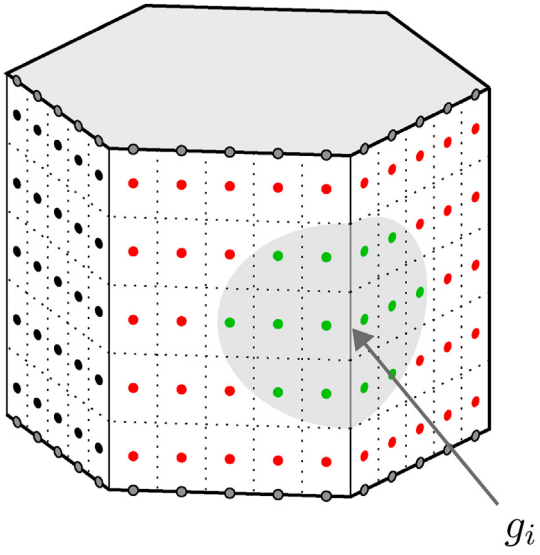

Fig. 5. Using the aim point reduction algorithm to reduce the number of aim points for heliostat group g_i. The dots on the receiver surface represent the aim points. For the heliostats of group g_i the black points are not visible, just the green and red aim points belong to the aim point set $\mathcal{A}_{g_i}$. With an aim point reduction size of 28%, the far away heliostat group is just allowed to aim on the green points of the set $\mathcal{A}_{g_i}^{\text{reduced}}$.

The union with the measurement points for the heat shield $\mathcal{M}^{\text{shield}}$ yields the set $\mathcal{M}$, see Fig. 1.

$$\mathcal{M} = \mathcal{M}^{\text{rec}} \cup \mathcal{M}^{\text{shield}} \tag{1}$$

The set of aim points $\mathcal{A}$, at which the heliostats can aim is generally a subset of the measurement points $\mathcal{M}^{\text{rec}}$, such that all peak fluxes

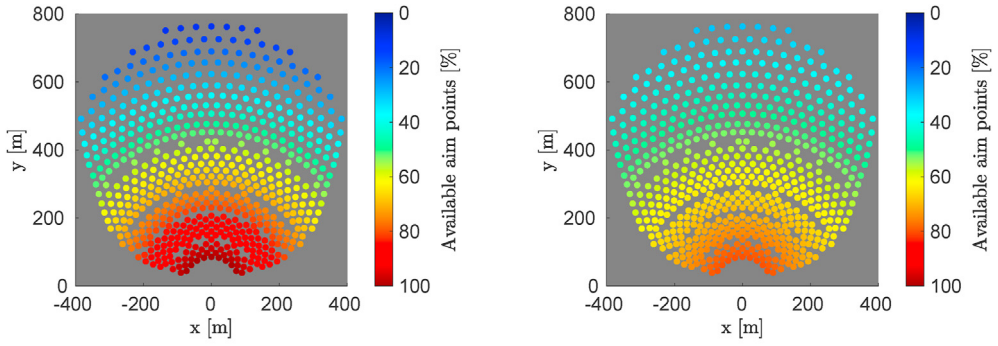

(a) $\xi_{\text{lower}} = 10\,\%$ and $\xi_{\text{upper}} = 100\,\%$. (b) $\xi_{\text{lower}} = 30\,\%$ and $\xi_{\text{upper}} = 80\,\%$.

Fig. 6. The further away, the stronger the reduction $\frac{|\mathcal{A}_h^{\text{reduced}}|}{|\mathcal{A}_h|}$ of the aim point set for each heliostat. The strength of reduction is shown by the color, here as example for the *PS10* central receiver system.

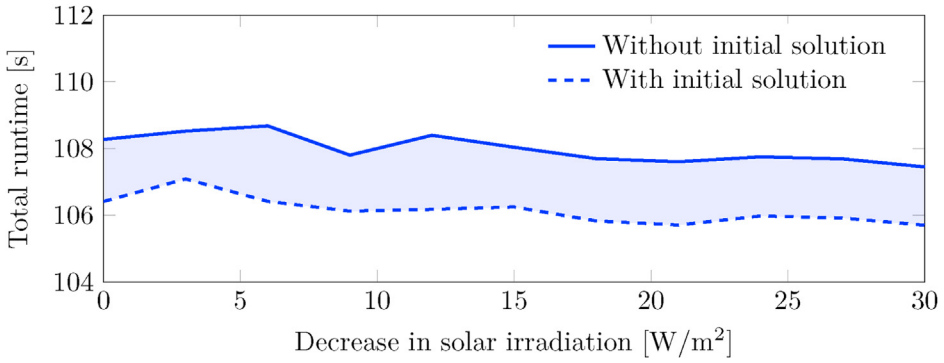

Fig. 7. Investigation of the runtime reduction for different changes of the solar irradiation between two time steps, while using the assignment of the first time step as initial solution for the second time step. The runtime reduction lies by about 1.5%.

on the receiver surface can be captured. As not every heliostat can see all aim points on the receiver surface, we denote the set of reachable aim points for heliostat $h \in \mathcal{H}$ with $\mathcal{A}_h$.

$$\mathcal{A}_h \subseteq \mathcal{A} \subseteq \mathcal{M}^{\text{rec}} \tag{2}$$

2.2. Allowed flux distribution

The receiver consists of several panels, each with parallel tubes for the heat carrying medium. The heat carrying medium cools the receiver material directly, such that high heat fluxes on the surface are possible without damaging the receiver. Following Sanchez et al. [15] the film temperatures of the heat transfer material limits the incident flux density. To ensure that the material of the receiver withstands the heat flux, a maximum *allowable flux distribution* (AFD) q_{AFD}^m for all measurement points $m \in \mathcal{M}^{\text{rec}}$ on the receiver surface can be computed [15].

The computations depend on the fluid temperature and the mass flow of the heat carrying medium, as changes in the mass flow locally impact the cooling effect on the receiver surface. As simplification, receiver manufacturers deliver precomputed AFD maps which just depend on the mass flow intensity $\chi^{\text{intensity}}$ according to the design point where the maximum possible mass flow with $\chi^{\text{intensity}} = 100\%$ is reached. With this simplified approach a large safety margin is considered, to cover the worst case scenario for all possible fluid temperatures. Thus, for different flow intensities the AFD maps are given, see Fig. 2 for an example. For intermediate mass flow intensities we use point-wise linear interpolation between two AFD maps.

As the heat shield around the receiver just consists of solid material, e.g. ceramics, a fixed value q_{shield} for maximum heat flux can be given for all measurement points $m \in \mathcal{M}^{\text{shield}}$ on the heat shield.

(a) Design point with flow intensity $\chi^{\text{intensity}} = 100\%$
(b) Flow intensity $\chi^{\text{intensity}} = 75\%$
(c) Flow intensity $\chi^{\text{intensity}} = 50\%$

2.3. Heat flux computation

The heat flux $q_{h,a}^m$ describes the power density in $\frac{\text{W}}{\text{m}^2}$ arriving at a measurement point $m \in \mathcal{M}$ for a heliostat $h \in \mathcal{H}$ aiming at aim point $a \in \mathcal{A}_h$. Approaches to compute the heat flux can be divided into the non-deterministic Monte Carlo based ray tracers [16–21] and the deterministic analytical ray tracers [21–25] which describe the reflected flux of a heliostat on a image plane orthogonal to the reflection direction by some two-dimensional function. In this work we utilize an analytical heat flux computation method based on the HFLCAL method [23], where heliostat $h \in \mathcal{H}$ aiming on aim point $a \in \mathcal{A}_h$ delivers a heat flux of

$$q_{h,a}^m = \frac{P_{h,a}}{2\,\pi\,\sigma_{h,a}^{\text{eff}}} \cdot \exp\left(-\frac{(x_a^m)^2 + (y_a^m)^2}{2\sigma_{h,a}^{\text{eff}}} \right) \cdot \left[\frac{1}{\text{m}^2}\right], \tag{3}$$

onto a measurement point $m \in \mathcal{M}$. $\sigma_{h,a}^{\text{eff}}$ is the effective error which

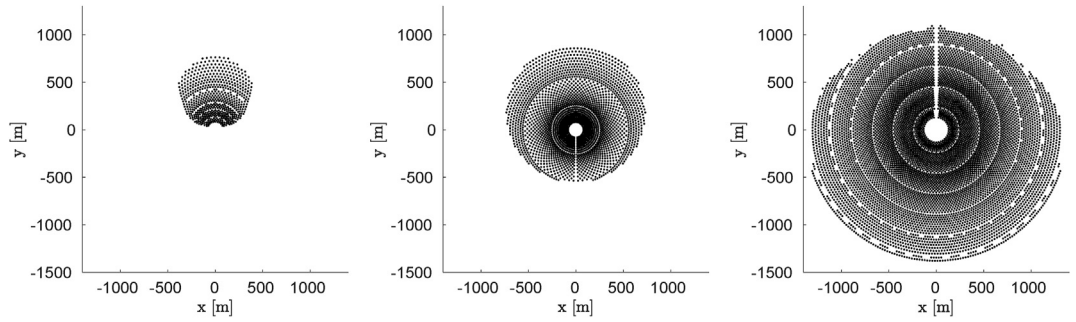

(a) Layout of *PS10* (b) Layout of *Gemasolar* (c) Layout of *Abengoa CRS*

Fig. 8. Heliostat field layouts for *PS10*, *Gemasolar* and *Abengoa CRS*. The tower with the receiver is positioned at the origin.

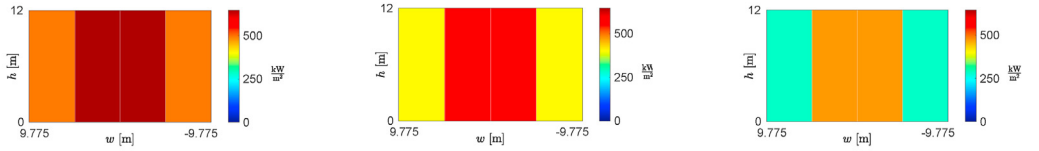

(a) Design point with flow intensity $\chi^{\text{intensity}} = 100\,\%$ (b) Flow intensity $\chi^{\text{intensity}} = 75\,\%$ (c) Flow intensity $\chi^{\text{intensity}} = 50\,\%$

Fig. 9. AFD maps for the *PS10* central receiver system for different flow intensities $\chi^{\text{intensity}}$ on the receiver surface. The *PS10* receiver consists of 4 panels.

Table 3
Data for the three central receiver systems *PS10*, *Gemasolar* and the *Abengoa CRS*.

	Symbol	Unit	*PS10*	*Gemasolar*	*Abengoa CRS*
Meteo parameters					
Sunshape error	σ^{sunshape}	mrad	2.35	2.35	2.35
Direct normal irradiation	I_{DNI}	$\frac{\text{W}}{\text{m}^2}$	950	950	950
Northern azimuth angle	γ^{solar}	deg	180	180	0
Altitude angle	θ^{solar}	deg	76	76	76
Heliostat parameters					
Number of heliostats	$\lvert\mathcal{H}\rvert$		624	2650	8600
Mirror surface area	A	m^2	121	115.7	138.7
Pedestal height	z^{pedestal}	m	5.17	5.68	7.10
Heliostat surface error	σ^{optical}	mrad	2.9	2.9	1.22
Reflectivity	$\eta_h^{\text{reflectivity}}$		0.88	0.93	0.92
Tracking error horizontal	$\sigma^{\text{tracking, hor}}$	mrad	1.3	1.3	0.71
Tracking error vertical	$\sigma^{\text{tracking, vert}}$	mrad	2.6	2.6	0.38
Receiver parameters					
Type			cavity	external	external
Number of horizontal panels			4	18	16
Receiver length	ℓ^{rec}	m	19.55	26.70	50.89
Receiver height	h^{rec}	m	12	10.6	18.5
Tower height	h^{tower}	m	115	140	230
Allowed heat flux	q_{AFD}	$\frac{\text{kW}}{\text{m}^2}$	see Fig. 9	see Fig. 2	see Fig. 10
Allowed heat flux (shield)	q_{shield}	$\frac{\text{kW}}{\text{m}^2}$	400	400	400

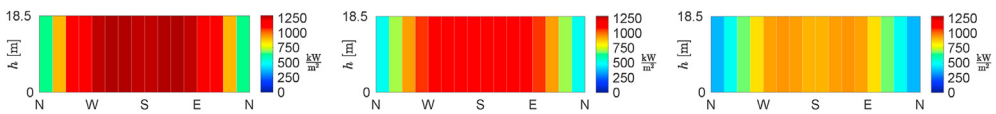

(a) Design point with flow intensity $\chi^{\text{intensity}} = 100\,\%$ (b) Flow intensity $\chi^{\text{intensity}} = 75\,\%$ (c) Flow intensity $\chi^{\text{intensity}} = 50\,\%$

Fig. 10. AFD maps for the *Abengoa CRS* central receiver system for different flow intensities $\chi^{\text{intensity}}$ on the receiver surface. The *Abengoa CRS* receiver consists of 16 panels.

considers imperfections of the mirror surface or tracking errors. It defines the distribution size and scales with the aim distance. x_a^m and y_a^m describe the horizontal and vertical distance of the measurement point from the aim point on the surface of the receiver.

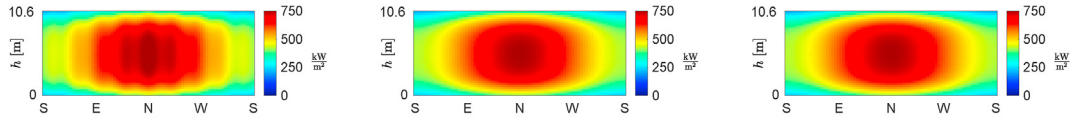

(a) $|\mathcal{M}^{\text{rec}}| = 9 \times 5$ (b) $|\mathcal{M}^{\text{rec}}| = 18 \times 7$ (c) $|\mathcal{M}^{\text{rec}}| = 36 \times 7$

Fig. 11. Investigation of the number of aim points $|\mathcal{A}|$ on the receiver surface of the power plant *Gemasolar*, which has 18 horizontal panels. While a too low resolution (a) delivers alternating peaks and troughs, higher resolutions result in a smooth behavior (c). The lowest resolution is chosen which still delivers a smooth behavior (b).

Table 4
Selected resolution of aim points and measurement points for the three power plants.

Receiver resolution	Symbol	*PS10*	*Gemasolar*	*Abengoa CRS*
Number horizontal points	$n_a^{\text{horiz}} = n_m^{\text{horiz}}$	12	18	32
Number vertical points	$n_a^{\text{vert}} = n_m^{\text{vert}}$	5	7	10

$P_{h,a}$ represents the amount of irradiation reflected from the heliostat towards the receiver. This total beam power considers the direct solar irradiance, cosine losses, atmospheric attenuation, surface reflectivity and shading efficiency. As an extension to the standard HFLCAL method, we add distortion depending on the angle with which the ideal heat flux beam hits the receiver surface and shadows based on the receiver shape. With these modifications the heat flux computation delivers more accurate results, especially for the cavity and external receiver [26].

For any given plant configuration it is possible to precompute all possible flux distributions $q_{h,a}$. The required memory space for the images depends on the number of heliostats, aim points and measurement points.

2.4. Aim point management system

In central receiver systems an *aim point management system* is the central unit for the dynamic computation and assignment of aim points for each heliostat. It collects meteorological data from the sensors in the solar field, runs the computation for finding an optimal aim point strategy and communicates to the control systems of the receiver and the heliostat field, see Fig. 3. Real-time dynamics like clouds or changes of the direct normal irradiation are considered by solving the aim point problem at discrete instances of time, which should be a couple of seconds apart under operating conditions. At each time step the following steps have to be proceeded:

1. Estimate the mass flow intensity $\chi^{\text{intensity}}$ of the receiver system:
   (a) At start-up the theoretical maximum possible flux can be estimated by virtually letting all heliostats aim on the center of their aim points. Shaded heliostats have a reduced contribution. The received theoretical power is reduced by 1–2% (depends on the configuration of the central receiver system) due to further spillage losses by the aiming strategy. The estimated mass flow intensity $\chi^{\text{intensity}}$ is given relative to the design point.
   (b) During operation, the flow intensity of the previous time step should be used and updated according to changes in the environment. Changes of the direct normal irradiation shall be considered linearly. For shadows of clouds in the heliostat field newly shaded heliostats and de-shaded heliostats shall linearly be considered. Cloud shadows can be detected by using a now-casting system [27].
2. Load the corresponding allowed flux map according to the mass flow intensity $\chi^{\text{intensity}}$, e.g. see Fig. 9. Between two given AFD maps point-wise linear interpolation is used.
3. Solve the aim point problem according to the in Section 3 formulated equation system.
4. Compute the delivered heat flux on the receiver surface which results from the solution of the aim point problem. Reversely determine the lowest possible AFD map for which all constraints are fulfilled and adjust the pump throughput of the plant accordingly.

In Section 5 a dynamic test case with a passing cloud throughout three different solar fields is drawn, using the aim point management system. It can be shown that the presented results are close to real-time.

3. Optimization problem formulation

We now present a linear formulation of the optimization problem for finding an optimal aiming strategy in central receiver systems based on the presented model. The objective is to maximize the total power received at the receiver surface while preventing dangerous flux peaks which would damage the receiver. This model is based on the formulation of Ashley et al. [10] and Kuhnke et al. [13] with the addition of the heat shield constraints and an updated constraint formulation.

3.1. Formulation of the optimization problem as an ILP

The optimization formulation consists of decision variables which the optimizer needs to set to reach an optimal objective function value while considering the given constraints for the choice of the decision variables. We want to find optimal assignments for the decision variables, which determine if heliostat $h \in \mathcal{H}$ aims at aim point $a \in \mathcal{A}_h$,

$$x_{h,a} \in \{0,1\} \; \forall \; h \in \mathcal{H}, \forall \; a \in \mathcal{A}_h. \tag{4}$$

$$\sum_{a \in \mathcal{A}} x_{h,a} \leq 1 \; \forall \; h \in \mathcal{H}. \tag{5}$$

The binary variable $x_{h,a}$ is equal to one if h aims at a and zero otherwise. Naturally each heliostat can only aim at most at one point, while we also allow to not utilize a heliostat at all. The objective is to maximize the total power received at all measurement points on the receiver surface. Therefore, we optimize the following objective function:

$$\max_x \sum_{m \in \mathcal{M}^{\text{rec}}} \sum_{h \in \mathcal{H}} \sum_{a \in \mathcal{A}} \left(A^m \cdot q_{h,a}^m \cdot x_{h,a} \right), \tag{6}$$

where $q_{h,a}^m$ is the heliostats' heat flux (3), and A^m represents the surface area assigned to this measurement point. Finally, the incoming heat flux is limited to q_{AFD}^m and q_{shield} for the receiver and heat shield respectively:

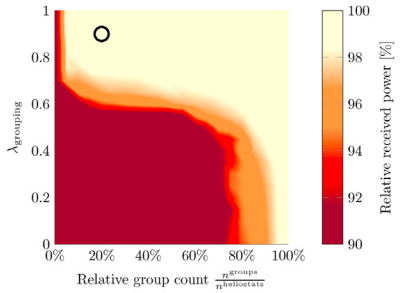

(a) Influence of heliostat grouping on optimiality for *PS10*.

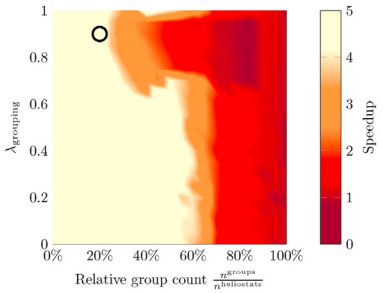

(b) Influence of heliostat grouping on runtime for *PS10*.

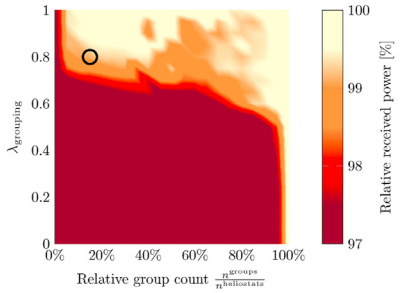

(c) Influence of heliostat grouping on optimiality for *Gemasolar*.

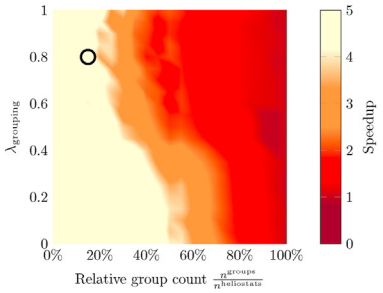

(d) Influence of heliostat grouping on runtime for *Gemasolar*.

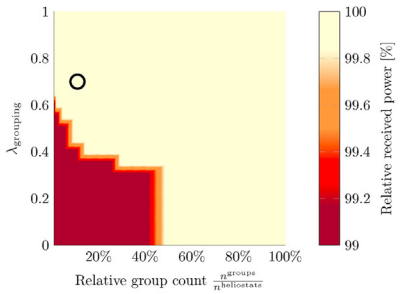

(e) Influence of heliostat grouping on optimiality for *Abengoa CRS*.

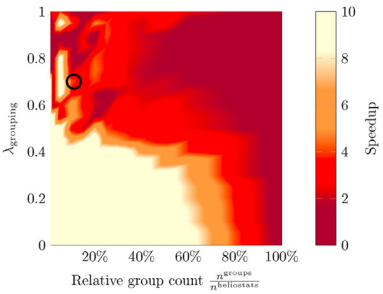

(f) Influence of heliostat grouping on runtime for *Abengoa CRS*.

Fig. 12. The influence of the grouping method $\lambda_{\text{grouping}}$ and the number of groups n^{groups} on the quality of the solution in (a), (c) and (e) and on the runtime in (b), (d) and (f). The optimality increases for larger n^{groups} and $\lambda_{\text{grouping}}$, while the runtime mainly depends on the group size. The black circle ◦ indicates the value selection from Table 5.

Table 5
Selected parameters for the heliostat grouping heuristic for the three power plants *PS10*, *Gemasolar* and *Abengoa CRS*. All parameters are chosen such that the optimality is larger than 99% while at the same time reaching a large speedup for the runtime.

Power plant	Relative group count $\frac{n^{\text{groups}}}{n^{\text{heliostats}}}$	Grouping method $\lambda_{\text{grouping}}$	Optimality	Runtime speedup
PS10	20%	0.9	99.41%	3.65
Gemasolar	15%	0.8	99%	5.25
Abengoa CRS	10%	0.7	99.37%	4.12

$$\sum_{h\in\mathcal{H}}\sum_{a\in\mathcal{A}} q^m_{h,a}\cdot x_{h,a} \le q^m_{\text{AFD}}\ \forall\ m\in\mathcal{M}^{\text{rec}}, \tag{7}$$

$$\sum_{h\in\mathcal{H}}\sum_{a\in\mathcal{A}} q^m_{h,a}\cdot x_{h,a} \le q_{\text{shield}}\ \forall\ m\in\mathcal{M}^{\text{shield}}. \tag{8}$$

The ILP presented here for the optimization of aiming strategies has $|\mathcal{H}|\cdot|\mathcal{A}|$ decision variables and $|\mathcal{H}|+|\mathcal{M}|$ constraints.

3.2. ILP solver

In general, an ILP is solved with the simplex and branch-and-bound or branch-and-cut algorithm [28]. There exist several software tools as Gurobi, CPLEX, SCIP, glpk, lpSolve and COIN-OR. As Gurobi[1] is a commercial software, it is to be expected that it outperforms the other non-commercial solver tools. CPLEX[2] provides a commercial alternative to Gurobi and is expected to deliver results in comparable timeframes. SCIP [29,30] claims to be one of the

[1] Gurobi Optimization, Version 9.0, http://www.gurobi.com.
[2] ILOG CPLEX Optimization Studio, CPLEX Version 12.9.0, https://www.ibm.com/products/ilog-cplex-optimization-studio.

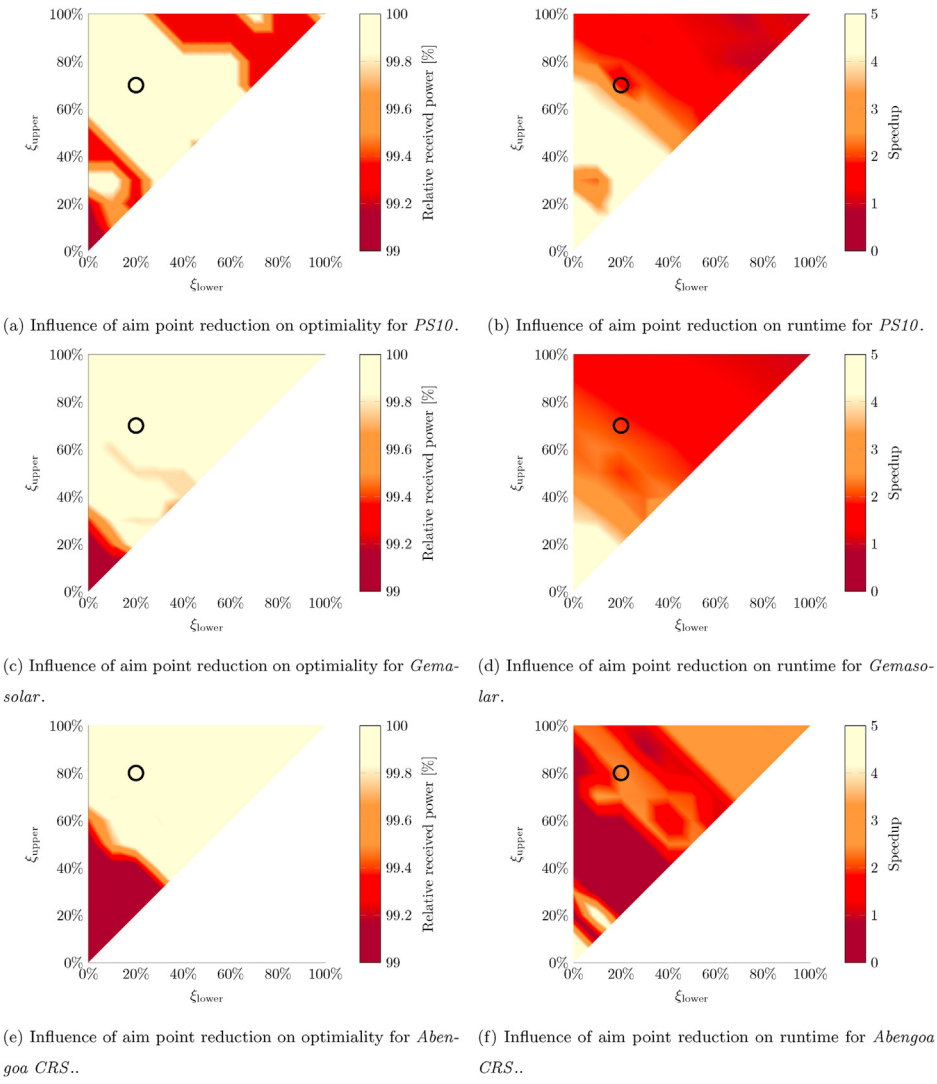

(a) Influence of aim point reduction on optimiality for *PS10*.

(b) Influence of aim point reduction on runtime for *PS10*.

(c) Influence of aim point reduction on optimiality for *Gemasolar*.

(d) Influence of aim point reduction on runtime for *Gemasolar*.

(e) Influence of aim point reduction on optimiality for *Abengoa CRS*..

(f) Influence of aim point reduction on runtime for *Abengoa CRS*..

Fig. 13. The influence of the aim point reduction by the two parameters ξ_{lower} and ξ_{upper} on the quality of the solution shown in (a), (c) and (e), and on the runtime shown in (b), (d) and (f). The optimality increases for larger ξ_{lower} and ξ_{upper}, while at the same time also the runtime is raised. As $\xi_{lower} \leq \xi_{upper}$, just results in the top left triangle are shown. The black circle ◦ indicates the value selection from Table 6.

Table 6
Selected parameters for the aim point reduction for the three power plants *PS10*, *Gemasolar* and *Abengoa CRS*. All parameters are chosen such that the optimality is larger than 99%, while at the same time a large speedup for the runtime can be achieved.

Power plant	Lower reduction amount ξ_{lower}	Upper reduction amount ξ_{upper}	Optimality	Runtime speedup
PS10	20%	70%	99.98%	1.23
Gemasolar	20%	70%	99.99%	1.91
Abengoa CRS	20%	80%	99.74%	2.45

Table 7
Verification data for the three central receiver systems *PS10*, *Gemasolar* and the *Abengoa CRS*. All unchanged parameters can be found in Table 3.

Power plant	Direct normal irradiation I_{DNI}	Northern azimuth angle γ^{solar}	Altitude angle θ^{solar}
PS10	$950\,\frac{W}{m^2}$	270 deg	20 deg
Gemasolar	$950\,\frac{W}{m^2}$	270 deg	20 deg
Abengoa CRS	$950\,\frac{W}{m^2}$	90 deg	20 deg

Table 8
Performance for the verification problem from Table 7 for the three central receiver systems *PS10*, *Gemasolar* and the *Abengoa CRS* using just one core on the CPU.

Power plant	Optimality	Speedup	Runtime
PS10	99.53%	12.11	0.2 s
Gemasolar	99.4%	10.46	3.2 s
Abengoa CRS	99.06%	8.96	114.3 s

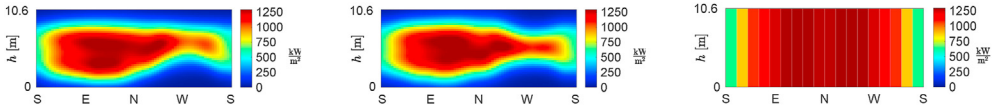

(a) Heat flux image from the solution for the original problem.

(b) Heat flux image from the solution for the reduced problem.

(c) Allowed flux distribution.

Fig. 14. Solutions for the verification problem for *Gemasolar*. The heat fluxes for the original problem formulation (a) and the reduced problem formulation (b) are similar and stay below the allowed heat flux distribution (c).

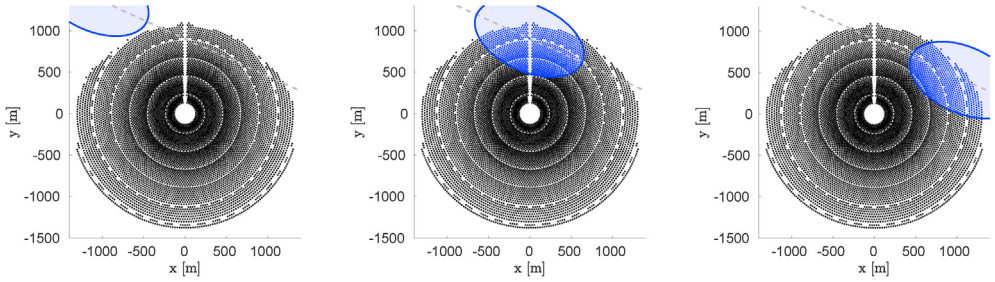

(a) Cloud position for $t = 0$ sec.

(b) Cloud position for $t = 60$ sec.

(c) Cloud position for $t = 120$ sec.

Fig. 15. Path of the cloud for the dynamic test case. Heliostat marked blue in (b) are obscured by the cloud and do not contribute to the heat flux image.

fastest non-commercial solvers for mixed integer programming and mixed integer nonlinear programming. glpk[3] (GNU Linear Programming Kit) is a package designed to solve linear programming and mixed integer programming problems. lpSolve[4] is a mixed integer linear programming solver which is based around the simplex and branch-and-bound algorithm. COIN-OR [31] (Common Optimization Interface for Operations Research) offers several tools in the field of operations research, one of them being the Cbc (Coin-or branch-and-cut) solver. An overview of all used solvers is given in Table 1.

We use irace [32] to automatically configure the large variety of parameters of the solvers, as e.g. SCIP offers 2425 parameters, over 100 of which have directly to do with the ILP solving algorithm. This tool tunes these parameters by iteratively running a given problem using different configurations. In Table 2 the run-time for finding the optimal aiming strategy for a test case of the *PS10* and *Gemasolar* central receiver system using the five different solvers is given. The criterion to stop the solution algorithm is set using the duality gap, which is a property defining the maximum possible difference between the best solution found so far and the upper bound for the optimum. An exhaustive search would decrease it to 0%, while in practice, a threshold for the gap is used as a termination criterion, we use a value of 5% for the tuning of our solvers. A detailed description of the remaining problem parameters is given in Section 5.

From Table 2 it can be seen that lpSolve and COIN-OR are not suitable for our kind of problem, as they need too much time to achieve a solution. SCIP and glpk manage to produce results in an acceptable time, while Gurobi is by far the fastest solver. It is to be expected that the solution time scales with the problem size for all solvers similarly. Due to this result, we use Gurobi for all our measurements in this work and decrease the termination criterion for the duality gap to 1% to achieve more accurate solutions. CPLEX also produces results in a comparable time and could be used alternatively to Gurobi.

4. Acceleration

Since the runtime of the optimization directly depends on the problem size, we investigate different methods to artificially reduce the number of $|\mathcal{A}|\cdot|\mathcal{H}|$ decision variables. The goal is to achieve a solution in significantly less time, while minimizing the impact of the reduction on the optimality of the solution. In the following we propose three different accelerations which can be used. While the first two aim on artificially reducing the number of regarded aim points and number of heliostats, the third approach focuses on the acceleration during a dynamic simulation.

4.1. Grouping of heliostats

To reduce the number of objects for which we need to find an aim point, we propose to create groups of heliostats, where all heliostats of one group simultaneously target the same aim point. Thus, instead of finding an aim point for every individual heliostat $h \in \mathcal{H}$ the problem changes to find an aim point for each group $g \in \mathcal{G}$. The set of n^{groups} groups is defined as

[3] GNU Linear Programming Kit, Version 4.65, https://www.gnu.org/software/glpk/glpk.html.

[4] lpSolve, Version 5.5, http://lpsolve.sourceforge.net/5.5/.

Table 9
The properties of the cloud used in the dynamic test case.

Cloud properties	Values
Start position	(-1100, 1400)
End position	(2000, 0)
Speed	20 m/s
Large half-axis	700 m
Small half-axis	400 m
DNI of the shadow	100 W/m^2

Table 10
The entry and exit time of the cloud shadow over the heliostat field for *PS10*, *Gemasolar* and the *Abengoa CRS*.

Power plant	Shadow entry	Shadow exit
PS10	$t = 29$ s	$t = 118$ s
Gemasolar	$t = 21$ s	$t = 134$ s
Abengoa CRS	$t = 5$ s	$t = 169$ s

$$\mathcal{G} = \left\{ g_i | i = 1, \ldots, n^{\text{groups}}, \quad g_i \subseteq \mathcal{H}, \quad \bigcup_i g_i = \mathcal{H}, \quad g_i \cap g_j = \varnothing \, \forall \, i \neq j \right\}, \tag{9}$$

while the groups are non-overlapping subsets of $\mathcal{H}$. To evaluate the heat flux reflected onto the receiver by a certain group g, we sum up the heat fluxes of its heliostats:

$$q^m_{g,a} = \sum_{h \in g} q^m_{h,a} \qquad \forall g \in \mathcal{G}. \tag{10}$$

The set of aim points the group $g \in \mathcal{G}$ can target is reduced to the intersection of the aim point sets visible from each heliostat of this group,

$$\mathcal{A}_g = \bigcap_{h \in g} \mathcal{A}_h \qquad \forall g \in \mathcal{G}. \tag{11}$$

To cluster heliostats into groups we propose to use the agglomerative clustering algorithm [33] which iteratively merges two clusters with the lowest *dissimilarity*, until the desired number of groups is achieved. As dissimilarity we propose two different functions:

- To keep the optimality high when grouping heliostats, one may ensure that not too many aim points per group are filtered out. Since heliostats from a similar circular sector have similar aim points sets, the angular difference is proposed as a dissimilarity function,

$$diss(h_i, h_j) = \alpha(p_i, p_j) = \arccos\left(\frac{\langle p_i, p_j \rangle}{\|p_i\|_2 \cdot \|p_j\|_2}\right), \tag{12}$$

with position vectors p_i and p_j of heliostats h_i and h_j, while the receiver is placed in the origin.

- One may also want to reduce the impact of clouds on the solution, which cover coherent parts of the heliostat field. Therefore, it is beneficial to have larger spatial distances between the heliostats of one group. As dissimilarity function the max-distance can be used,

$$diss(h_i, h_j) = -\|p_i - p_j\|_2. \tag{13}$$

To compute the dissimilarity of two heliostat groups, the maximum pair-wise dissimilarity of heliostats from the two groups is used. The resulting heliostat groups from the angular dissimilarity function (12) consist of many heliostats in close proximity, see Fig. 4a, while the max-distance dissimilarity function (13) creates widely spread out groups as displayed in Fig. 4c. To find a middle ground, a combined dissimilarity function can be used,

$$diss(h_i, h_j) = \lambda_{\text{grouping}} \cdot \left(\frac{\alpha(p_i, p_j)}{\pi}\right)^2 - (1 - \lambda_{\text{grouping}}) \cdot \frac{\|p_i - p_j\|_2}{\max_{k,l} \|p_k - p_l\|_2} \tag{14}$$

with weighting $\lambda_{\text{grouping}} \in [0, 1]$ between angular and max-distance dissimilarity function. Additional terms are used for normalizing the separate dissimilarity functions, while we also square the angular difference term to punish low aim point set overlaps more. The groups resulting from a combined dissimilarity function with $\lambda_{\text{grouping}} = 0.7$ are shown in Fig. 4b. This resulting groups are more diffuse while the aim point sets within a group overlap broadly.

In the case study in Section 5 for all three central receiver systems good choices for $\lambda_{\text{grouping}}$ and n^{groups} are presented.

4.2. Reduction of allowable aim points

To further reduce the problem size, we propose to reduce the individual sets of aim points the heliostats can target. Thus, while the initial aim point resolution with the total set $\mathcal{A}$ of all aim points stays unchanged, for each heliostat $h \in \mathcal{H}$ we develop a reduced aim

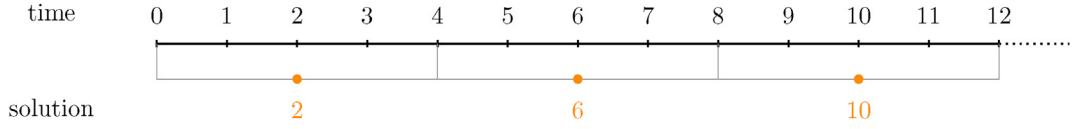

Fig. 16. In every center of a time interval (•) a solution is computed which lasts for the whole interval. In this example a time step of 4 s is shown. Nowcasting allows to compute solutions of future weather scenarios.

Table 11
Optimality for different time steps for the three central receiver systems *PS10*, *Gemasolar* and the *Abengoa CRS*.

Power plant	Optimality		
	4 s time interval	10 s time interval	14 s time interval
PS10	99.99% (using 1 core)	99.99% (using 1 core)	99.99% (using 1 core)
Gemasolar	99.99% (using 1 core)	99.91% (using 1 core)	99.86% (using 1 core)
Abengoa CRS	–	99.15% (using 12 cores)	98.34% (using 8 cores)

point set $\mathcal{A}_h^{\text{reduced}} \subseteq \mathcal{A}_h$.

Heliostats which are far away from the receiver tend to aim towards the receiver center, as their flux image on the receiver surface is larger than those of closer heliostats. We use this property to reduce the number of aim points. The further away, the stronger the reduction for each heliostat. In Fig. 5 the reduced aim point set is illustrated.

For a heliostat group $g_i \in \mathcal{G}$ the mean distance to the tower is given by

$$\text{dist}(g_i) = \frac{1}{|g_i|} \cdot \sum_{h \in g_i} \|p_h\|_2 \in [\text{dist}_{\min}, \text{dist}_{\max}], \tag{15}$$

where p_h denotes the position vectors of heliostats h around the tower at the origin. The group's mean distance ranges from $\text{dist}_{\min}$ to $\text{dist}_{\max}$, which is defined by the closest and furthest heliostat. The reduction of the aim point set is given by the distance ratio between a defined lower ξ_{lower} and upper ξ_{upper} reduction amount,

$$\frac{|\mathcal{A}_{g_i}^{\text{reduced}}|}{|\mathcal{A}_{g_i}|} = \xi_{\text{upper}} - \frac{\text{dist}(g_i) - \text{dist}_{\min}}{\text{dist}_{\max} - \text{dist}_{\min}} \cdot (\xi_{\text{upper}} - \xi_{\text{lower}}). \tag{16}$$

In Fig. 6 we use the *PS10* central receiver system for demonstrating different relative aim point set sizes. The lower reduction amount ξ_{lower} shall not be zero to avoid nearly empty aim point sets for the furthest heliostats.

In the case study in Section 5 for all three central receiver systems good choices for the parameters ξ_{lower} and ξ_{upper} are presented.

4.3. Acceleration with initial solution

In practice, the aiming strategy is used as part of a dynamic aiming management system (Section 2.4), where the aim point problem is solved in a series of time steps to adjust to meteorological changes. A re-usage of prior knowledge can help to accelerate the solving process. The similarity of the aim point solutions from two consecutive time steps is expected to be high and depends on the temporal step size and the speed of meteorological changes.

We propose to use the aim point assignment of the previous time step as initial solution for the next time step. This will accelerate the solving step, as a close-to-optimal solution helps the underlying optimization method to discard worse solutions earlier. To test the general effectivity of this approach, we compare the runtime for solving an aim point problem with and without usage of an initial solution. As originating time step we use a solar irradiation of 950 W/m^2 for the *Gemasolar* plant.

In Fig. 7 the runtime reduction is shown for different drops in the solar irradiation. It can be seen that using an initial solution reduces the runtime by about 1.5%. We conclude that providing an initial solution to the aiming strategy problem does not necessarily result in significantly faster computation times. The reason that the speedup is not larger, is likely due to the difficulty of lowering the upper bound for the best possible solution. The solver also cannot rely on any further data to stay valid and has to verify the optimality of the given initial solution again or find a better solution.

5. Case study

In this section, we present a case study which applies the presented formulations for the optimization of aiming strategies introduced in Section 3 and its accelerations in Section 4. As test fields we usethree different power plant configurations, which vary from hundreds to several thousand heliostats considering two different receiver systems:

- The *PS10* power plant [34] is located near Seville in Spain With 624 heliostats and a cavity receiver (which consists of four rectangular panels aligned as four sides of a nonagon) the power plant generates an electrical power output of 11 MW_{el}.
- The *Gemasolar* Thermosolar Plant [35] is located in the province of Seville in Spain. The central receiver system consists of 2650 heliostats which are spread around a cylindric external receiver. It produces an electrical power output of 19.9 MW_{el}.
- The *Abengoa CRS* power plant in Chile is still in planning stage. It has 8600 heliostats in total and uses a cylindric external receiver. It will produce an electrical power output of 220 MW_{el}.

The heliostat field layouts of all central receiver systems are shown in Fig. 8, a list of all parameters is given in Table 3, and the maps of allowed heat fluxes q_{AFD} can be seen in Figs. 2, 9 and 10.

In the following we present the setup of the experiments and specifications about the implementation. First we determine a suitable aim point resolution for the different central receiver systems in Section 5.1. Then in Section 5.2 and 5.3 the optimal acceleration settings for the heliostat grouping and aim point reduction. The overall accelerations are then compared to the results of the original formulation in Section 5.4. In Section 5.5 a dynamic test case with a passing cloud throughout all three solar fields is drawn. It can be shown that the presented results are close to real-time. Finally, a discussion of the results can be found in Section 5.6.

5.1. Investigation of the aim point resolution

As defined in Section 2 we need to find a horizontal and vertical number of receiver points for $\mathcal{M}$ and $\mathcal{A}$. As introduced in Section 2, we choose the same resolution for both $\mathcal{M}^{\text{rec}}$ and $\mathcal{A}$, as a further increase in measurement points does not improve the accuracy of the solution process.

The grid resolution is chosen such that a smooth heat flux distribution can be obtained. For this investigation we propose to let every heliostat $h \in \mathcal{H}$ aim on every aim point $a \in \mathcal{A}_h$ with $\frac{1}{|\mathcal{A}_h|}$-partial solar irradiation. The grid resolution is iteratively increased until a smooth behavior in the eyeball norm is reached. For the number of points in horizontal direction it is considered that the chosen number of aim points are a multiple (or divisor) of the number of receiver panels. In Fig. 11 this procedure can be seen for *Gemasolar*.

For the following investigations we choose the receiver resolutions as listed in Table 4. The measurement points for the heat shield $\mathcal{M}^{\text{shield}}$ are selected correspondingly on the border of the receiver, see also Fig. 1.

5.2. Investigation of the heliostat grouping

As introduced in Section 4, the optimality of the solution and the runtime acceleration depend on the number of groups n^{groups} and the grouping method, which is controlled via $\lambda_{\text{grouping}} \in [0, 1]$. Our goal is to find parameters for all three plants which reduce the runtime as much as possible while keeping the solution quality over 99%. In Fig. 12 for all three central receiver systems different grouping configurations and the resulting optimality and runtime are shown. It can be seen that a relative group size of $\frac{n^{\text{groups}}}{n^{\text{heliostats}}} < 30\,\%$

(due to runtime reasons) and a grouping method value of $\lambda_{grouping} > 0.6$ (due to optimality reasons) shall be chosen.

Table 5 shows the chosen values for $\lambda_{grouping}$ and n^{groups} for all three power plants, which we will use for the following investigations. The parameters are chosen such that no runtime spikes appear in their immediate neighborhood, to not rely on an outlier. Altogether, an optimality of 99% or higher can be reached, while the speedup is between 3.65 and 5.25.

5.3. Investigation of the aim point reduction

As introduced in Section 4 the aim point reduction depends on the two parameters ξ_{lower} and ξ_{upper}, which describe the reduction of the aim point set in dependency of the distance from heliostat to receiver. The goal is again to keep an optimality of more than 99% while achieving the highest possible speedup.

Fig. 13 shows the coarse nature of the runtime and optimality decrease for all three power plants. It can be seen that aim point reduction has a non-neglectable impact on the runtime of the solution, while the optimality just slightly changes. Table 6 shows the chosen values for ξ_{lower} and ξ_{upper}, which we will use for the following investigations. The chosen values capture the steepest speedup while not entering a critical zone where the problem becomes hard to solve and the runtimes as well as optimality might fluctuate, depending on the test case. Altogether, an optimality of 99.7% or higher can be reached, while the speedup is at maximum at about 2.5.

5.4. Overall optimality and speedup

To determine the overall optimality and speedup for the above chosen heliostat grouping and aim point reduction parameters in Sections 5.2 and 5.3, we change the sun position according to Table 7. The resulting overall performance can be found in Table 8.

The overall optimality stays higher than 99% while the achieved speedups is about 10. While the runtimes for *PS10* and *Gemasolar* are just a few seconds, the large solar field *Abengoa CRS* needs about 114 s. For larger power plants as *Abengoa CRS*, parallel computation can be used to reach real-time, 12 core-processors can compute a solution about every 10 s.

In Fig. 14, the resulting heat flux for *Gemasolar* is displayed, using the original formulation in 14 (a) and the reduced problem formulation in 14 (b). In the central part of the receiver the heatflux is spread out a bit more for the reduced problem, which is where the slight drop in optimality originates from. Of course, both flux maps stay below the allowed flux distribution at every measurement point from Fig. 14 (c).

5.5. Dynamic test case with passing cloud

To investigate the performance of the accelerated aiming strategy in a dynamic setting, we simulate a cloud passing over the heliostat field. Fig. 15 shows the path of the cloud for *Abengoa CRS*, the same path is used for all three plants. Our test case covers a time of 172 s, as we use a cloud moving at 20 m/s. The cloud settings for this test case are shown in Table 9 and the time frames in which the shadow covers at least one heliostat are given in Table 10.

Heliostats covered by the cloud shadow reflect a reduced heat flux onto the receiver surface. Therefore the optimal aim points for the heliostats change over the course of the simulation, as a lower number of strong irradiated heliostats leads to more freedom in the aim point choices.

We consider having an exact nowcasting system, as e.g. demonstrated in Nouri et al. [36], to know the future cloud movement. At every time step a new heliostat assignment is computed, which holds for the whole time interval, see Fig. 16. We investigate how strong the quality of the solution depends on the temporal step size, while as reference we compute the solution at every second for the entire duration of the cloud passing over the heliostat field.

With growing time intervals the risk of exceeding the AFD rises, such that larger safety margins for the AFD must be considered. We set the safety margin proportional to the number of critical heliostats, which enter the cloud shadow before the solution time or leave afterwards. In Table 11 the assignment quality for different time steps is shown, compared to the reference solution where in every second a solution is computed. As *PS10* and *Gemasolar* have a runtime of less than 4 s (see Table 8) we can simply just use one core. For *Abengoa CRS* we need to consider multicore parallelization, where in parallel computations the assignment problem at different time points in the future are solved. Altogether, the optimality decreases for larger time intervals, which is for 14 s time intervals still higher than 98%.

5.6. Discussion of the results

The developed acceleration techniques for the aim point optimization are presented within a case study using three real central receiver systems. The grid resolution on the receiver surface is chosen such that a smooth behavior of the receiver flux is reached.

It is shown that grouping of heliostats can reduce the runtime substantially. In our cases speedups in the order of 4 are achieved without a significant loss in optimality. The grouping parameters have to be chosen carefully though, as the parameter $\lambda_{grouping}$, which controls the grouping method, heavily impacts the optimality for lower values. A higher speedup of 10 can be achieved by additionally reducing the number of aim points for each individual heliostat group, without a further loss of optimality. Altogether the optimality of the accelerated method stays above 99%.

A dynamic test case simulates a scenario of passing clouds and shows that heliostat updates with a frequency of 4 s for *PS10* and *Gemasolar* deliver results close to the optimum. For the larger power plant *Abengoa CRS* we show that using multicore parallelization with 12 cores delivers results with an optimality of 99%. The presented approach is efficient and flexible enough to be applied in real central receiver systems.

6. Conclusion

This work presents an approach for the acceleration of the aiming strategy optimization in central receiver systems with the goal to increase the efficiency of the system in dynamic application. We formulate the aim point optimization problem as an integer linear program (ILP). The runtime to compute the solution depends on the size of the heliostat field, which in its original formulation needs minutes. Several accelerations are proposed to reduce the runtime to a few seconds while preserving an overall optimality of higher than 99% compared to the global optimum.

In a case study we use three cental receiver systems with different heliostat sizes and different receiver technologies. We show the impact of the acceleration on the runtime and the optimality. For the optimal alignment in dynamic test cases we propose an aim point management system, which controls the heliostat alignment and the receiver mass flow automatically. As input a nowcasting system is used to allow optimizations at future weather situations.

The developed aiming strategy is ready to be used in a real field test which remains as future step of this work. As further improvement for the application in dynamic situations receiver sensors shall be considered which allow the computation of more

dynamic AFD maps. This would lead to a further reduction in the safety margins which directly increases the efficiency.

CRediT authorship contribution statement

N. Speetzen: Conceptualization, Methodology, Software, Writing – original draft, Visualization. **P. Richter:** Conceptualization, Methodology, Writing – original draft, Supervision, Project administration.

Declaration of competing interest

The authors declare that they have no known competing financial interests or personal relationships that could have appeared to influence the work reported in this paper.

Acknowledgments

The authors thank Markus Schramm from Abengoa S.A. for providing us data for the case study.

References

[1] T. Dellin, M. Fish, C. Yang, User's manual for DELSOL 2: a computer code for calculating the optical performance and optimal system design for solar-thermal central-receiver plants, in: Tech. rep., Sandia National Labs., Albuquerque, NM (USA), Sandia National Labs., Livermore, CA (USA), 1981, https://doi.org/10.2172/6082347.

[2] F. García-Martín, M. Berenguel, A. Valverde, E. Camacho, Heuristic knowledge-based heliostat field control for the optimization of the temperature distribution in a volumetric receiver, Sol. Energy 66 (5) (1999) 355–369, https://doi.org/10.1016/s0038-092x(99)00024-9.

[3] B.D. Kelly, Advanced thermal storage for central receivers with supercritical coolants, in: Tech. Rep., Abengoa Solar Inc., lakewood, CO, 2010, https://doi.org/10.2172/981926. Report No. DOE/GO18149.

[4] M. Astolfi, M. Binotti, S. Mazzola, L. Zanellato, G. Manzolini, Heliostat aiming point optimization for external tower receiver, Sol. Energy 157 (2017) 1114–1129, https://doi.org/10.1016/j.solener.2016.03.042.

[5] J. García, Y. Chean Soo Too, R. Vasquez Padilla, A. Beath, J.-S. Kim, M. E. Sanjuan, Multivariable closed control loop methodology for heliostat aiming manipulation in solar central receiver systems, J. Sol. Energy Eng. 140 (3). doi: 10.1115/1.4039255.

[6] F.J. Collado, J. Guallar, A two-parameter aiming strategy to reduce and flatten the flux map in solar power tower plants, Sol. Energy 188 (2019) 185–189, https://doi.org/10.1016/j.solener.2019.06.001.

[7] B. Belhomme, R. Pitz-Paal, P. Schwarzbözl, Optimization of heliostat aim point selection for central receiver systems based on the ant colony optimization metaheuristic, J. Sol. Energy Eng. 136 (1) (2014), 011005, https://doi.org/10.1115/1.4024738.

[8] S.M. Besarati, D.Y. Goswami, E.K. Stefanakos, Optimal heliostat aiming strategy for uniform distribution of heat flux on the receiver of a solar power tower plant, Energy Convers. Manag. 84 (2014) 234–243, https://doi.org/10.1016/j.enconman.2014.04.030.

[9] L. Oberkirsch, D. M. Quinto, P. Schwarzbözl, B. Hoffschmidt, Gpu-based aim point optimization for solar tower power plants, Sol. Energy:10.1016/j.solener.2020.11.053.

[10] T. Ashley, E. Carrizosa, E. Fernández-Cara, Optimisation of aiming strategies in solar power tower plants, Energy 137 (2017) 285–291, https://doi.org/10.1063/1.5067041.

[11] T. Ashley, E. Carrizosa, E. Fernández-Cara, Continuous optimisation techniques for optimal aiming strategies in solar power tower plants, Sol. Energy 190 (2019) 525–530, https://doi.org/10.1016/j.solener.2019.08.004.

[12] P. Richter, F. Kepp, C. Büsing, S. Kuhnke, Optimization of robust aiming strategies in solar tower power plants, in: SolarPACES 2018: International Conference on Concentrating Solar Power and Chemical Energy Systems, AIP Publishing LLC, AIP Publishing, 2019, https://doi.org/10.1063/1.5117557.

[13] S. Kuhnke, P. Richter, F. Kepp, J. Cumpston, A. M. Koster, C. Büsing, Robust optimal aiming strategies in central receiver systems, Renew. Energy: 10.1016/j.renene.2019.11.118.

[14] P. Richter, N. Speetzen, Accelerated aiming strategy in central receiver systems using integer linear programming. AIP Conference Proceedings, AIP Publishing LLC, 2021.

[15] A. Sánchez-González, M.R. Rodríguez-Sánchez, D. Santana, Allowable solar flux densities for molten-salt receivers: input to the aiming strategy, Results in Engineering 5 (2020) 100074, https://doi.org/10.1016/j.rineng.2019.100074.

[16] M.J. Blanco, J.M. Amieva, A. Mancillas, The tonatiuh software development project: an open source approach to the simulation of solar concentrating systems, in: Computers and Information in Engineering, ASMEDC, 2005, https://doi.org/10.1115/imece2005-81859.

[17] P.L. Leary, J.D. Hankins, User's guide for MIRVAL: a computer code for comparing designs of heliostat-receiver optics for central receiver solar power plants, in: Tech. Rep, Sandia Laboratories, 1979, https://doi.org/10.2172/6371450.

[18] T. Wendelin, Soltrace: a new optical modeling tool for concentrating solar optics, in: ASME 2003 International Solar Energy Conference, American Society of Mechanical Engineers, 2003, pp. 253–260, https://doi.org/10.1115/isec2003-44090.

[19] B. Belhomme, R. Pitz-Paal, P. Schwarzbözl, S. Ulmer, A new fast ray tracing tool for high-precision simulation of heliostat fields, J. Sol. Energy Eng. 131 (3). doi: 10.1115/1.3139139.

[20] M. Izygon, P. Armstrong, C. Nilsson, N. Vu, Tiesol – a GPU-based suite of software for central receiver solar power plants, Proceedings of the SolarPACES conference.

[21] P. Richter, G. Heiming, N. Lukas, M. Frank, SunFlower: a new solar tower simulation method for use in field layout optimization, in: SolarPACES 2017: International Conference on Concentrating Solar Power and Chemical Energy Systems, AIP Publishing LLC, AIP Publishing, 2018, https://doi.org/10.1063/1.5067217.

[22] F. Biggs, C. Vittitoe, The Helios Model for the Optical Behavior of Reflecting Solar Concentrators, Tech. Rep., Sandia Labs., Albuquerque, NM (USA), March 1979, https://doi.org/10.2172/6273705.

[23] P. Schwarzbözl, R. Pitz-Paal, M. Schmitz, Visual HFLCAL - a software tool for layout and optimisation of heliostat fields. Proceedings of the 15th SolarPACES Conference, 2009, pp. 1–8.

[24] A. Sánchez-González, D. Santana, Solar flux distribution on central receivers: a projection method from analytic function, Renew. Energy 74 (2015) 576–587, https://doi.org/10.1016/j.renene.2014.08.016.

[25] B. L. Kistler, reportA User's Manual for Delsol3: a Computer Code for Calculating the Optical Performance and Optimal System Design for Solar Thermal Central Receiver Plants, Sandia National Laboratories, Sandia Report No. SAND86-8018doi:10.2172/7228886.

[26] N. Speetzen, Accelerated Aiming Strategy for Central Receiver Systems by Integer Linear Optimization Using Heuristics, Bachelor Thesis, RWTH Aachen University, 2017.

[27] P. M. Kuhn, D. Garsche, S. Wilbert, B. Nouri, N. Hanrieder, C. Prahl, L. Zarzalejo, J. Fernández, A. Kazantzidis, T. Schmidt, et al., Shadow-camera based solar nowcasting system for shortest-term forecasts, Meteorol. Z.:10.1127/metz/2019/0954.

[28] R.E. Gomory, An algorithm for integer solutions to linear programs. Tech. Rep., Princeton IBM Mathematics Research, 1958.

[29] A. Gleixner, M. Bastubbe, L. Eifler, T. Gally, G. Gamrath, R.L. Gottwald, G. Hendel, C. Hojny, T. Koch, M.E. Lübbecke, S.J. Maher, M. Miltenberger, B. Müller, M.E. Pfetsch, C. Puchert, D. Rehfeldt, F. Schlösser, C. Schubert, F. Serrano, Y. Shinano, J.M. Viernickel, M. Walter, F. Wegscheider, J.T. Witt, J. Witzig, The SCIP Optimization Suite 6.0, Technical Report, Optimization Online, July 2018.

[30] A. Gleixner, M. Bastubbe, L. Eifler, T. Gally, G. Gamrath, R.L. Gottwald, G. Hendel, C. Hojny, T. Koch, M.E. Lübbecke, S.J. Maher, M. Miltenberger, B. Müller, M.E. Pfetsch, C. Puchert, D. Rehfeldt, F. Schlösser, C. Schubert, F. Serrano, Y. Shinano, J.M. Viernickel, M. Walter, F. Wegscheider, J.T. Witt, J. Witzig, The SCIP Optimization Suite 6.0, ZIB-Report 18-26, Zuse Institute Berlin, July 2018.

[31] R. Lougee-Heimer, The common optimization interface for operations research: promoting open-source software in the operations research community, IBM J. Res. Dev. 47 (1) (2003) 57–66, https://doi.org/10.1147/rd.471.0057.

[32] M. López-Ibáñez, J. Dubois-Lacoste, L. Pérez Cáceres, T. Stützle, M. Birattari, The irace package: iterated racing for automatic algorithm configuration, Operations Research Perspectives 3 (2016) 43–58, https://doi.org/10.1016/j.orp.2016.09.002.

[33] A. Lukasová, Hierarchical agglomerative clustering procedure, Pattern Recogn. 11 (5–6) (1979) 365–381, https://doi.org/10.1016/0031-3203(79)90049-9.

[34] R. Osuna, R. Olavarria, R. Morillo, M. Sánchez, F. Cantero, V. Fernández-Quero, P. Robles, T. López, A. Esteban, F. Céron, et al., PS10, construction of a 11MW solar thermal tower plant in Seville, Spain, in: Proceedings of the 12th SolarPACES Conference, A4–S3, 2006, pp. 1–8.

[35] J. Burgaleta, S. Arias, D. Ramirez, Gemasolar, the first tower thermosolar commercial plant with molten salt storage, in: Proceedings of the 17th SolarPACES Conference, 2011.

[36] B. Nouri, P. Kuhn, S. Wilbert, C. Prahl, R. Pitz-Paal, P. Blanc, T. Schmidt, Z. Yasser, L.R. Santigosa, D. Heineman, Nowcasting of dni maps for the solar field based on voxel carving and individual 3d cloud objects from all sky images, in: AIP Conference Proceedings, vol. 2033, AIP Publishing LLC, 2018, https://doi.org/10.1063/1.5067196.